Intensity images and statistics from numerical simulation of wave propagation in 3-D random media

J. M. Martin and Stanley M. Flatté

An extended random medium is modeled by a set of 2-D thin Gaussian phase-changing screens with phase power spectral densities appropriate to the natural medium being modeled. Details of the algorithm and limitations on its application to experimental conditions are discussed, concentrating on power-law spectra describing refractive-index fluctuations of the neutral atmosphere. Inner and outer scale effects on intensity scintillation spectra and intensity variance are also included. Images of single realizations of the intensity field at the observing plane are presented, showing that under weak scattering the small-scale Fresnel length structure of the medium dominates the intensity scattering pattern. As the strength of scattering increases, caustics and interference fringes around focal regions begin to form. Finally, in still stronger scatter, the clustering of bright regions begins to reflect the large-scale structure of the medium. For plane waves incident on the medium, physically reasonable inner scales do not produce the large values of intensity variance observed in the focusing region during laser propagation experiments over kilometer paths in the atmosphere. Values as large as experimental observations have been produced in the simulations, but they require inner scales of the order of 10 cm. Inclusion of an outer scale depresses the low-frequency end of the intensity spectrum and reduces the maximum of the intensity variance. Increasing the steepness of the power law also slightly increases the maximum value of intensity variance.

I. Introduction

Propagation of waves in random media has applications in a variety of situations of scientific or engineering interest: acoustic waves in the ocean; radio in the interstellar, interplanetary, and ionospheric plasmas; seismic waves in the earth; light waves in the atmosphere. The effect of variations in the refractive index of a medium on waves propagating through it is well characterized if the intensity fluctuations are weak, i.e., intensity variance normalized by the mean intensity is <0.3.[1] Furthermore, asymptotic results for very strong scattering are also available.[2] Between these limiting cases lies an intermediate region containing interesting phenomena, such as focusing of waves to produce large values of intensity variation; the intensity statistics in this region are not well known. Simulations such as those described in this paper are effective tools for probing this region but are limited in application to only moderately strong scatter conditions. Thus they complement the theoretical results valid for the asymptotic region of very strong scatter and provide a means to evaluate the accuracy and range of validity of the low-order terms of approximate theoretical expansions.[2–5]

Two-dimensional simulations of wave propagation in random media have previously been used to analyze sound propagation in the ocean[6,7] and radio propagation through the ionosphere,[8,9] both of which are highly anisotropic media well suited to such an approach. The atmosphere is not so anisotropic, and only a full 3-D simulation can display accurately scintillation which results from propagation through it. We present results based on such simulations run on the CRAY XM-P supercomputer at the San Diego Supercomputer Center. The first section briefly describes the algorithm, which is well known and used for all 2-D simulations referred to above and also by the only previous 3-D simulation in the literature.[10] We also discuss the limits on the applicability of the simulations.

In Sec. III results of the simulations are presented for intensity variance, intensity spectra, and images of single realizations of intensity in the observation

The authors are with University of California, Santa Cruz, Physics Department, Santa Cruz, California 95064.

Received 26 August 1987.
0003-6935/88/112111-16$02.00/0.

plane. Media with various refractive-index spectra are examined (pure power law, power law with inner/outer scale, Gaussian), and the results of variation of the medium parameters are discussed. The images dramatically show the effects of refractive and diffractive phenomena only hinted at by the statistical quantities. Finally, we compare our results to a theoretical computation of Whitman and Beran[5] and consider the use of an equivalent thin screen to represent an extended medium, as suggested by Booker *et al.*[11]

II. Simulation Algorithm

If we restrict propagation to the forward (x) direction and write the wave field as

$$\phi = \psi \exp(-ikx), \tag{1}$$

then ψ satisfies the parabolic approximation to the wave equation[12]

$$2ik\partial_x\psi + \nabla_\perp^2\psi + 2k^2n_1\psi = 0, \tag{2}$$

where $k = 2\pi/\lambda$, the wavenumber, $n_1 = n - \langle n\rangle$, the deviation of the refractive index from its mean which is a stochastic quantity, and $\nabla_\perp^2 \equiv \partial_{yy} + \partial_{zz}$. More precise conditions in which this approximation may be made are detailed elsewhere[7,13–15]; the important implication of these conditions is that we may divide the extended random medium into slabs of some thickness δ_x, each introducing an independent random contribution to the wave phase, but essentially no change in amplitude. Amplitude variations build up by diffraction over many δ_x. For simplification of the description which follows, we assume a homogeneous medium modeled by identical uniformly spaced phase screens. This condition is not required; indeed nonuniformly spaced phase screens modeling a medium which may slowly change its statistical properties in the direction of propagation is a situation ideally suited to simulation, as such a medium is generally difficult to deal with analytically.

With these assumptions, we calculate the correlation function and spatial spectrum of phase variations which will be needed to specify the statistics of each phase screen. Since no diffraction is allowed in each slab, we may write the phase correlation function as the geometric optics result:

$$B_\theta(\rho_1,\rho_2) = k^2\int\int_0^{\delta_x}\langle n_1(x,\rho_1)n_1(x',\rho_2)\rangle\,dx\,dx'$$

$$= k^2\delta_x A_n(\rho_1 - \rho_2), \tag{3}$$

where ρ is a 2-D position vector (y,z), and B_θ is the correlation between phases arriving at ρ_1 and ρ_2. In simplifying Eq. (3) we have used the assumption that $\delta_x > L$, the correlation length of the irregularities.[2] $A_n(r)$ is the correlation function of refractive-index variations in the y-z plane and may be expressed in terms of the spatial spectrum of irregularities $\Phi_n(\kappa)$ (Ref. 1) as

$$A_n(\rho) = 2\pi\int\int_{-\infty}^{\infty}\Phi_n(\kappa_x = 0,\kappa)\exp(i\kappa\cdot\rho)d^2\kappa. \tag{4}$$

Therefore, the relationship between the phase spectrum for each screen and refractive-index spectrum is

$$\Phi_\theta(\kappa) = 2\pi k^2\delta_x\Phi_n(\kappa_x = 0,\kappa). \tag{5}$$

Each phase screen is created by the well-known method[7,16] of filtering white Gaussian noise to obtain a random field with the desired second-order statistics: an $N\times N$ field of pseudorandom complex numbers $A_{jn} + B_{jn}$ [A_{jn} and B_{jn} independent on $N(0,1)$] is multiplied by $\Delta_\kappa^{-1}\sqrt{\Phi_\theta(j\Delta_\kappa,n\Delta_\kappa)}$ and inverse transformed by 2-D discrete Fourier transform (DFT) to yield the desired random phase field $\theta_1 + i\theta_2$, where $\Delta_\kappa = 2\pi/N\Delta$ is the wavenumber increment and Δ is the sampling interval. This method produces two phase screens for each transform, each with Gaussian statistics and continuous phase at the screen edges. Sample screens generated by this technique are shown in the following section.

Propagation of the wave field from screen to screen is accomplished by solving Eq. (2) for $n_1 = 0$ in the spectral domain. Let $\Psi(x,\kappa)$ be the 2-D Fourier transform of $\psi(x,y,z)$. Then the transform of Eq. (2) is

$$\frac{\partial\Psi(x,\kappa)}{\partial x} = -i\frac{\kappa^2}{2k}\Psi(x,\kappa), \tag{6}$$

which has the solution

$$\Psi(x',\kappa) = \Psi(x,\kappa)\exp\left[-i\frac{\kappa^2(x'-x)}{2k}\right]. \tag{7}$$

Thus the procedure to propagate a wave in a random medium over $\delta_x = x' - x$, with $\psi(x-,\rho)$ being the field impinging on the screen at x, is

(a) $\psi(x,\rho) = \psi(x-,\rho)\exp[i\theta(\rho)]$,

(b) DFT $\psi(x,\rho)$ to $\Psi(x,\kappa)$,

(c) $\Psi(x'-,\kappa) = \Psi(x,\kappa)\exp\left[-i\frac{\kappa^2(x'-x)}{2k}\right]$.

(d) inverse DFT $\Psi(x'-,\kappa)$ to $\psi(x'-,\rho)$.

The procedure is repeated for all screens until the observing plane is reached. It has been observed that this algorithm is the discrete analog to the path integral method of wave scattering analysis and, therefore, is an exact solution to the parabolic wave equation within the restrictions imposed by the finite screen size and sampling interval.[13,14]

For the computations, all lengths in the problem have been scaled by the sampling interval Δ. Under this scaling, the spectrum of any quantity becomes

$$\hat{W}(\hat{\kappa}) = \frac{1}{\Delta^2}W(\hat{\kappa}/\Delta), \tag{8}$$

where $\hat{W}$ and $\hat{\kappa}$ are the spectra and wavenumber in the normalized coordinates. The sampling interval in these coordinates becomes unity, and the wavenumber interval $\hat{\delta}_\kappa = 2\pi/N$. Therefore, spectra of real quantities, such as intensity and phase, will be over the wavenumber range $(0,\pi)$. To translate back to the unnormalized world for comparison to experiment, we just invert Eq. (8). In the remainder of this section, we discuss the conditions in which simulations may accurately model scattering behavior and the range of ap-

plicability of a given simulation with a given parameter set.

It is clear from Eq. (7) that the only geometric parameters which must be specified for this procedure are the Fresnel length corresponding to the normalized interscreen distance δ_x: $r_f = \sqrt{\delta_x/k}$ and the number of screens n_s. We will see that for n_s large enough, the only scattering parameters needed to specify the simulation relevant to a given experiment are the strength parameters σ_1^2 (Ref. 17) or U (Ref. 18) and the parameters required to specify the shape of Φ_n. U is defined as the intensity variance calculated by using the Rytov theory, and σ_1^2 is U for the special case of a pure power law medium with index $\alpha + 2$; they are accurate estimates of the normalized intensity variance

$$\sigma_I^2 = \frac{\langle I^2 \rangle}{\langle I \rangle^2} - 1, \tag{9}$$

only when scattering is weak. For an extended medium with homogeneous isotropic statistics and plane wave propagation,

$$U = 4\pi k^2 R \int_0^\infty \Phi_n(0,\kappa) \left[1 - \frac{\sin(\kappa^2 R_f^2)}{\kappa^2 R_f^2} \right] d\kappa, \tag{10}$$

where $R_f^2 = R/k$ and $\kappa^2 = \kappa_y^2 + \kappa_z^2$ and

$$\sigma_1^2 = C(\alpha) C_n^2 k^{2-\alpha/2} R^{1+\alpha/2}, \tag{11}$$

where

$$C(\alpha) = \frac{2\Gamma(1-\alpha/2)\Gamma(1+\alpha)}{\alpha(1+\alpha/2)} \cos\left(\frac{\pi\alpha}{4}\right) \sin\left[\frac{(\alpha-1)\pi}{2}\right]. \tag{12}$$

The most important limitation on the applicability of the simulations is the finite spatial dynamic range imposed by the maximum available grid size. If the spatial spectrum of intensity is to be calculated, all important components of the spectrum must be contained in the spectral window defined by the minimum wavenumber π/N and the maximum wave number π. A schematic drawing of the intensity spectrum is shown in Fig. 1 for large U—the spectral range between $\kappa_{\min}$ and $\kappa_{\max}$ must be included in the simulation spectral bandwidth to obtain an accurate representation of the intensity fluctuations. As U increases, the separation between $\kappa_{\min}$ and $\kappa_{\max}$ increases until it is greater than the available bandwidth. At this point the simulation breaks down due to severe aliasing problems.

To estimate the required dynamic range $R_\kappa = \kappa_{\max}/\kappa_{\min}$, we use the high- and low-frequency asymptotic approximations of Codona *et al.*[2] for the case of plane wave propagation through pure power-law media. These results must be modified if a different medium spectrum is used.

The high-frequency approximation to the intensity correlation function is

$$C_0^{\mathrm{hf}}(\rho) = \Gamma_2(\rho,R)\Gamma_2^*(\rho,R) = \exp[-D(\rho)], \tag{13}$$

where the plane-wave phase structure function $D(\rho)$ is defined by

$$D(\rho) = 4\pi k^2 R \int_{-\infty}^{\infty} [1 - \cos(\rho \cdot \kappa)] \Phi_n(\kappa_x,\kappa) d^2\kappa. \tag{14}$$

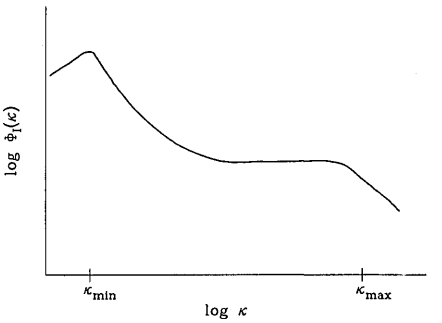

Fig. 1. Schematic representation of $\Phi_I(\kappa)$ in strong scattering conditions. $\kappa_{\max}$ and $\kappa_{\min}$ are wavenumber limits defining simulation spectral window requirements.

Therefore, the high-frequency approximation to the intensity spectrum is[19,20]

$$\Phi_I^{\mathrm{hf}}(\kappa) = \frac{1}{(2\pi)^2} \int_{-\infty}^{\infty} \exp[-D(\rho)] \exp(-i\rho \cdot \kappa) d^2\rho, \tag{15}$$

which has itself a low-frequency asymptote

$$\frac{\rho_0^2 \Gamma\left(\frac{2}{\alpha}\right)}{2\pi\alpha}, \tag{16}$$

where ρ_0 is the correlation length of the field defined by $D(\rho_0) = 1$. The high-frequency asymptote to Φ_I^{hf} is proportional to the refractive-index spectrum $\Phi_n(\kappa)$:

$$4\pi k^2 R \Phi_n(\kappa_x = 0,\kappa). \tag{17}$$

For pure power-law spectra $[\Phi_n(\kappa) \propto \kappa^{-\alpha-2}]$ with $1 \le \alpha < 2$, the intersection of these asymptotes is approximately at $\kappa = \rho_0^{-1}$. We will define $\kappa_{\max}$ as that wave number for which Eq. (17) is 10 dB lower than the flat level defined by Eq. (16):

$$\kappa_{\max} = \rho_0^{-1} 10^{\frac{1}{\alpha+2}}. \tag{18}$$

The low-frequency approximation to the intensity spectrum is[2,19]

$$\Phi_I^{\mathrm{lf}}(\kappa) = 4\pi k^2 \Phi_n(\kappa) \int_0^R \exp\left[-\int_0^R d\left[\frac{\kappa}{k} h(x,x')\right] dx \right] \times \sin^2\left[\frac{\kappa^2(R-x')}{2k}\right] dx', \tag{19}$$

where

$$h(x,x') = \begin{cases} R - x' & x < x', \\ R - x & x > x', \end{cases}$$

and $d(\Delta\rho)$ is the phase-structure function density.[21] The form of $\Phi_I^{\mathrm{lf}}(\kappa)$ is shown schematically in the left half of Fig. 1—it is increasing for $\kappa < \kappa_0$, then decreases exponentially for $\kappa > \kappa_0$. Typically, <1% of the intensity variation is contained in the spectral region $[0,\kappa_0]$, so if we set $\kappa_{\min} = \kappa_0$, almost all the spectral energy will be contained in the region $[\kappa_{\min},\kappa_{\max}]$. We substitute the pure power-law spectrum and structure function into Eq. (19) and find

$$\kappa_0 = \frac{k}{R}\left[\frac{\Gamma(1+\alpha/2)}{B(\alpha)k^2 C_n^2 R}\right], \tag{20}$$

which is equivalent to q^* of Goshelashvily and Shishov.[19]

So the required spatial bandwidth is

$$R_\kappa = 2 \cdot 10^{\frac{1}{\alpha+2}} \left[\frac{B(\alpha) k^{2-\frac{\alpha}{2}} C_n^2 R^{1+\frac{\alpha}{2}}}{\Gamma\left(1+\frac{\alpha}{2}\right)} \right]^{\frac{2}{\alpha}}$$

$$= 2(\sigma_1^2)^{\frac{2}{\alpha}} 10^{\frac{1}{\alpha+2}} \left[\frac{1+\frac{\alpha}{2}}{2\alpha\Gamma\left(1+\frac{\alpha}{2}\right)\cos\frac{\pi\alpha}{4}} \right]^{\frac{2}{\alpha}}, \quad (21)$$

which is only a function of σ_1^2 and α. For the simulations described here, with 512×512 screens, the maximum allowable bandwidth is 256. Thus, for $\alpha = 5/3$, the maximum σ_1^2 which may be accommodated is 14.2, which we have rounded to 15. It is clear that simulations with this screen size can never model scintillations in the asymptotic region of very strong scattering. In fact, even with 1024×1024 screens, the largest possible σ_1^2 is only 25. Clearly, simulations are most suited to analyzing scattering behavior in the transition region between the weak and saturated scattering regimes.

In addition to limits on the spatial bandwidth, the simulation parameters must be chosen so that $\hat{\kappa}_{\min} > \pi/N$ and $\hat{\kappa}_{\max} < \pi$. This requirement effectively constrains the normalized total Fresnel length $\hat{R}_f = \sqrt{n_s}\hat{r}_f$ to some value which sets $\hat{\kappa}_{\max} = \pi$ and $\hat{\kappa}_{\min} = \pi/N$ when U attains its maximum value. For U less than the maximum, this value for $\hat{R}_f$ is also satisfactory, as $\kappa_{\max}$ and $\kappa_{\min}$ are monotonically increasing and decreasing functions of U, respectively.

To model an extended medium, we have assumed that no intensity fluctuations are produced over the distance δ_x and that we can model the effect of the medium are purely an addition of phase. When the number of screens is finite, this is not strictly true, but we may impose the condition that the scattering be weak over the interscreen distance, i.e., $\sigma_I^2(\delta_x) < 0.1$. If the simulation is to represent an extended medium even in weak scatter when $\sigma_I^2(R) < 0.1$, we must in addition require the path to be sampled often enough. This condition is met by requiring that <10% of the total scintillation be allowed to take place over the interscreen distance, i.e., $\sigma_I^2(\delta_x) < 0.1\sigma_I^2(R)$. Thus, for a given value of U over the whole path, these conditions determine a minimum n_s and, therefore, a maximum value for the interscreen Fresnel distance $\hat{r}_f$.

For the Kolmogorov power law ($\alpha = 5/3$), the above considerations yield $\hat{R}_f = 5.0$, $n_s = 20$ or greater, and $\hat{r}_f = 1.12$ or less. Clearly the same simulation can be used to model any extended medium experiment with a given σ_1^2 and α regardless of the actual wavelength, propagation distance, and strength of scattering. It can also be shown[17] that when inner and outer scales are included, the important parameter is the ratio of inner or outer scale to the Fresnel length.

We have found that inner and outer scales affect intensity statistics significantly only when their values are within about an order of magnitude of the Fresnel length R_f, which spatial dynamic range is covered by the simulation 512×512 mesh. The effects of inner and outer scales outside the range of $(10R_f, 0.1R_f)$ are very small, and for simulation purposes the medium spectrum may be modeled as a pure power law in the high- or low-frequency regions, respectively. With regard to inner scale effects, both Frehlich[22] and Fante[17] predict theoretically <2% difference in σ_I^2 between zero inner scale and $0.1R_f$ for U less than 20.

The boundary conditions imposed by use of the DFT method of wave propagation and screen generation have already been mentioned: continuity of phase and amplitude at the edges of the screens. Imposition of this condition eliminates spurious diffraction which can be generated by phase or amplitude discontinuities. (Buckley[8] refers to this phenomenon as circular correlation and notes its salutary effect.) Thus the only edge effect we encounter is aliasing at high frequencies for large U.

The code we are using was developed on a VAX-11/750 but could only run 256×256 screens due to memory limitations—a single-screen propagation experiment took 7 min to run. When time on a CRAY became available, we ported the code, making only a minimal effort to vectorize, and used the FFT from the OMNILIB library. A speedup factor of ~200 was obtained, and much of the work presented in this paper was done with the algorithm in this form. Finally, using a multiple parallel FFT routine written by Oscar Buneman of Stanford University, and forcing vectorization wherever possible, the processing time has been reduced by another factor of 4, yielding a total speedup of 800 over the VAX. Presently, a propagation experiment with twenty 512×512 screens and ten realizations takes ~4.5 min. It is this computational speed which has made possible the relatively complete exploration of parameter space, which we will describe.

As with every simulation, it is difficult to be sure of the accuracy of the results in interesting conditions—the simulations are designed to probe regions of parameter space for which analytic tools are inadequate. The accuracy of the simulations must be checked in conditions for which analytic or numerical results have been obtained. We find that in weak scattering conditions, our simulations agree with results from Rytov theory.[1] We have also compared the first-order low-frequency approximation and the zeroth-order high-frequency approximation to simulation results. The results are shown in Fig. 2 for an extended pure power law medium, $\alpha = 1.7$, $U = 0.1$, 1.0, and 10.0. It is clear that asymptotically in wavenumber, the approximations agree with the simulation results.

To further check our results in another limiting case, we compared simulation of propagation through a single phase screen with numerical calculations using the exact theory[18,23] by Hinson[24] for $\alpha = 1.7$ and $U = 0.1$, 1.0, and 10.0. These results appear in Fig. 3, and the good agreement obtained is apparent. The smooth curves are Hinson's calculations, and the rougher curves are the simulation results averaged over ten

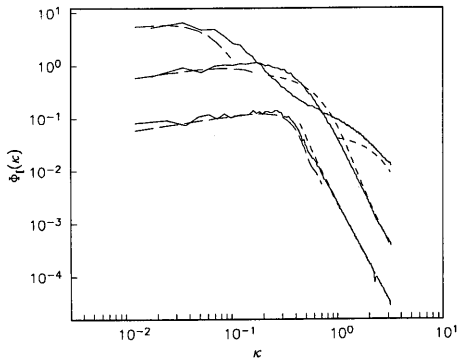

Fig. 2. Comparison of simulations vs low-frequency (long dash) and high-frequency (short dash) asymptotic theory of Codona *et al.* for extended medium: $\alpha = 1.7$, and $U = 0.1$, 1.0, and 10.0.

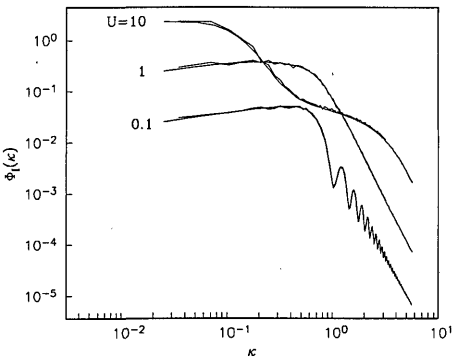

Fig. 3. Comparison of single-screen simulation results with calculations of Hinson for $\alpha = 1.7$ and $U = 0.1$, 1.0, and 10.0.

medium realizations and over azimuth in κ-space to reduce variance.

III. Results

In this section we present both statistics and pictures of intensity variations induced on a plane wave by propagation through random media described by (a) a pure power law over the entire spatial wavenumber spectrum, (b) a power law with inner scale cutoff, (c) a power law with outer scale limit, and (d) a Gaussian medium with a single scale. All media described in this paper are isotropic; anisotropic media could be included with an increase in the number of realizations. Isotropy also allows averaging spectra over all directions in κ space, producing a substantial reduction in variance especially at higher wavenumbers. All spectra presented in this paper are the result of averaging ten independent realizations, then azimuthally averaging.

A. Pure Power Law

The pure power-law approximation to a refractive-index fluctuation spectrum is appropriate for media possessing an extended inertial range compared to scale sizes measured by experiment, e.g., the solar wind density fluctuations.[25] For the pure power law, we write

$$\Phi_n(\kappa) = K(\alpha) C_n^2 \kappa^{-\alpha-2}, \tag{22}$$

where

$$K(\alpha) = \frac{\Gamma(\alpha+1)}{4\pi^2} \sin\left[(\alpha-1)\frac{\pi}{2}\right], \tag{23}$$

which is the standard Kolmogorov spectrum for $\alpha = 5/3[K(5/3) = 0.033]$.[1,20] A sample phase screen realization generated from this spectrum is shown in Fig. 4—the brightness of each pixel in the image is proportional to the phase difference the screen imposes on the incoming wave at that point. (If there were no fluctuations, the image would be uniformly the brightness in the middle of the scale at the top.) One can see that even with this rather steep power law, the substantial fine structure is apparent.

After passing through twenty phase screens like the one in Fig. 4, σ_I^2 and $\Phi_I^2(\hat{\kappa})$ were calculated for varying

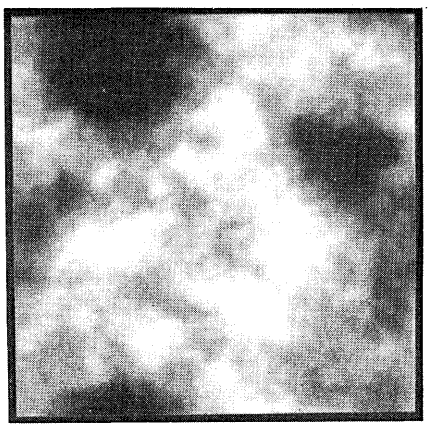

Fig. 4. Sample realization of a phase screen for a pure power law, $\alpha = 1.7$. Note the presence of both strong large-scale variation and small-scale filamentary structure.

strength of irregularities, keeping the geometry (R_f) constant. Intensity variances as a function of U are given in Fig. 5(a) for three values of the power law: $\alpha = 2.0$, 1.7, and 1.0. The peaks in the σ_I^2 curves all occur at $U = 4$ or 5, and the size of the peak increases with increasing power law. Apparently the smoother screens (less fine structure compared with large-scale structure) corresponding to larger α are more effective at focusing the radiation, producing larger and sharper intensity peaks.

Figures 5(b), (c), and (d) show intensity spectra corresponding to conditions before the peak in $\sigma_I^2(U = 1.0)$ at the peak ($U = 5.0$) and past the peak ($U = 10.0$). For U of unity, the spectra clearly show $\kappa^{4-\alpha-2}$ and $\kappa^{-\alpha-2}$ dependences for low and high wavenumbers, but for U of 10, these asymptotic regions have moved out of the spectral window due to the separation of refractive and diffractive wavenumbers discussed in the first section. Some aliasing is also present in the $U = 5$ and $U = 10$ spectra but only in the last half octave; this degree of aliasing does not cause significant errors in calculating σ_I^2. Note also the progression in the region $0.1 < \hat{\kappa} < 1.0$: for $U = 1$ the spectra are convex, then flat at $U = 5$, and concave at $U = 10$. The values of U for which the spectra possess minimal curvature in this region seem to correspond to the points of maximal intensity variance.

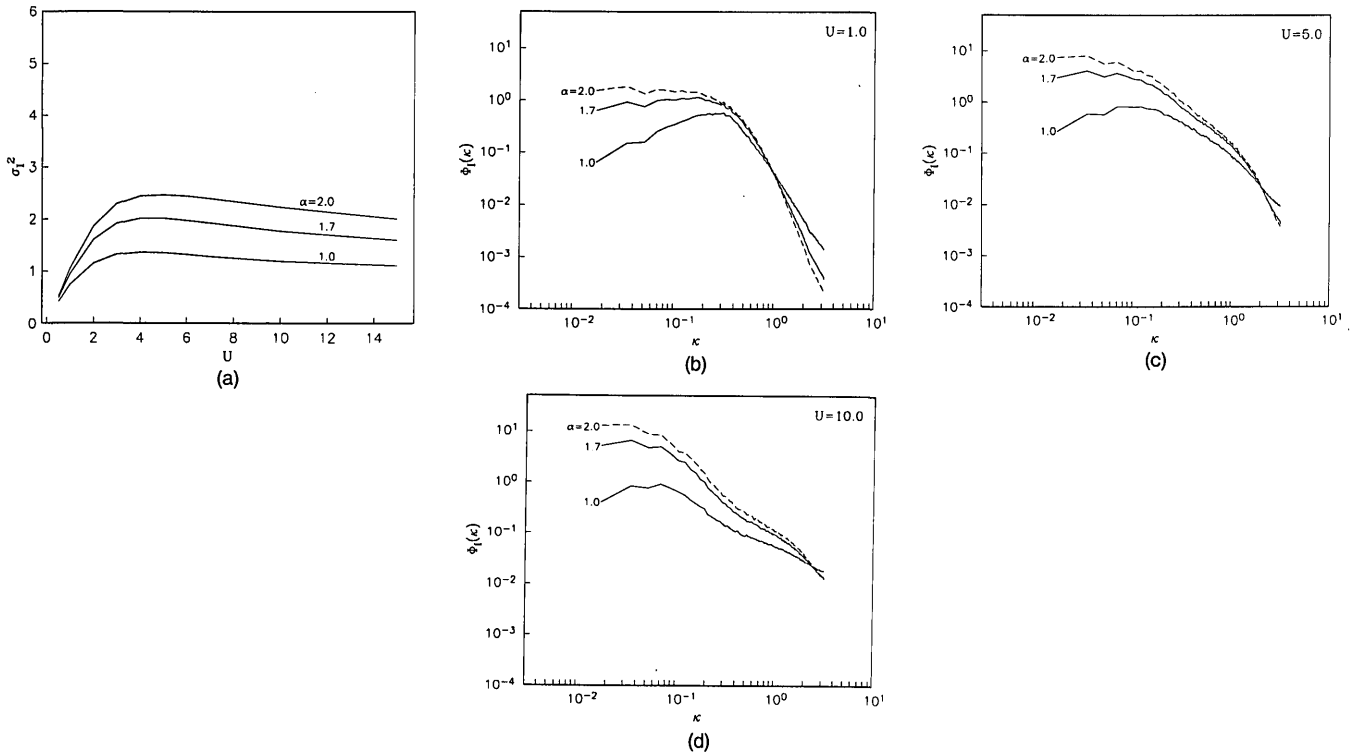

Fig. 5. Intensity statistics for pure power laws (α = 1.0, 1.7, and 2.0) for (a) intensity variance as a function of U; (b) intensity spectra for U = 1.0 describing conditions before the peak in σ_I^2; (c) intensity spectra at the maximum σ_I^2, U = 5.0; and (d) intensity spectra for U = 10.0 in the declining region of (a). U is varied by changing strength of medium fluctuations, keeping geometry constant.

A sequence of intensity images for increasing U is shown in Fig. 6, starting with weak scattering (U = 0.01). Each image represents the intensity results for a single realization of the 3-D medium with the intensity scale given at the right. Intensity values larger than the maximum shown were clipped to the maximum, and the mean intensity for all images is unity. This value is of course quite dark for the images with I_{max} = 10.

Figure 6(a) shows the results for weak scattering—not much large-scale structure, just slight variations from the mean gray value. The scale of variation which is most pronounced here is the Fresnel scale of about five samples. When U is increased to unity [Fig. 6(b)], small bright pointlike areas appear connected by dimmer (but still brighter than average) linear regions. The bright regions begin to cluster for U = 5 [Fig. 6(c)], and structures like fringes appear. This image corresponds to the maximum of intensity variance. If we allow the strength of scattering to increase by another factor of 2, we find the clustering of bright points has increased in magnitude and in area. The dominant clustering scale in Fig. 6(d) appears to be at about eighty samples ($\hat{\kappa}$ = 0.04), which corresponds to a wave number near the peak of the intensity scintillation spectrum [Fig. 5(d)], i.e., near κ_0, the wavenumber corresponding to the refractive scale. Also the fringe-like regions have been severely broken up and are not as apparent as in Fig. 6(c).

It seems that small-scale irregularities in the medium do most of the focusing and defocusing, as can be seen by the small scale of the intensity fluctuations in the images; the effect of the larger scale refractive-index variations when the propagation is described by strong scattering is to concentrate or diffuse the small-scale effects and thus either enhance or decrease the intensity variations over large-scale areas. We describe a test of this suggestion in Sec. III.C.

B. Inner Scale

When the inner scale cutoff of refractive-index fluctuations and the Fresnel length of the experiment are the same order of magnitude, the effect of the inner scale on intensity fluctuations may no longer be ignored. This is certainly the case for atmospheric propagation of 0.63-μm laser light over distances of a few kilometers, which yields a Fresnel length of ~1 cm, while the inner scale of atmospheric turbulence in the boundary layer near the ground is ~0.3–1 cm.[26] To model the spectrum of irregularities in this case, we use

$$\Phi_n(\kappa) = K(\alpha) C_n^2 \kappa^{-\alpha-2} \exp(-\kappa^2 \beta^2/4), \tag{24}$$

where the medium inner scale l_0 defined by the intersection of short-lag and long-lag approximations to the structure function of the fluctuations is 2.95β for α = 5/3.[1,20] We do not include the dissipation spectrum considered in more complete models of atmospheric turbulence,[27] and we will show results only for the

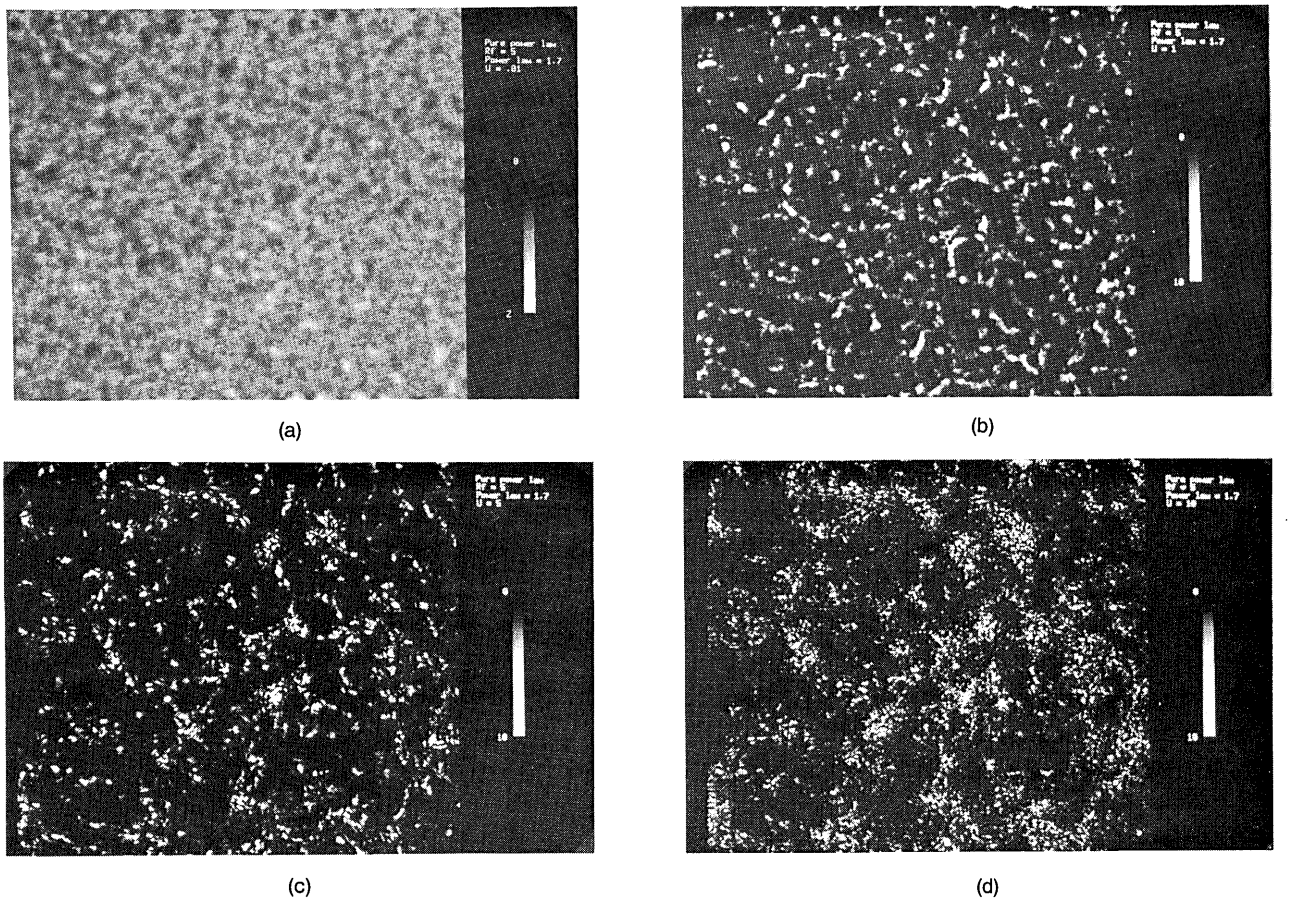

Fig. 6. Images of intensity for one realization of the 3-D pure power-law medium with $\alpha = 1.7$: (a) $U = 0.01$; (b) $U = 1.0$; (c) $U = 5.0$; and (d) $U = 10.0$. Intensity range is hard limited from 0 to 10, and the mean intensity is unity for all images.

Kolmogorov power law of 5/3. Figure 7 shows one phase screen generated from the spectrum Eq. (24) with $\beta = R_f/3$. Note that, compared with the pure power-law case of Fig. 4, the phase fluctuations are much smoother; as expected, the high spatial frequency structure has been removed by the high-frequency cutoff near $1/\beta$.

Theoretical calculations of the effect of a finite inner scale on intensity or log-amplitude variance suggest that an increase in σ_I^2 is expected with increasing l_0/R_f.[17,26] The two-scale calculations of Whitman and Beran[5] and the thin-screen calculations of Frehlich[22] also predict such an increase, so there is little doubt of the direction of the inner-scale effect. The question is the magnitude of the increase, especially in the region of the intensity variance peak, where the asymptotic theories are not valid. The results of our simulations are shown in Fig. 8(a) for $\beta = 1.6$, 5.0, and 15.0 (for all these runs, $\hat{R}_f = 5.0$).

The abscissa is the intensity variance U computed using the Rytov approximation.[28] The change in U here is produced by altering the strength of fluctuations C_n^2 rather than by propagating over a larger distance. The geometry in all runs was constant; thus these results pertain to running a propagation experiment over the same path but at different times, assuming constant l_0. If the propagation distance is changed instead of the strength of fluctuations, the peak value of the intensity variance is increased, all geometrical factors being equal. For example, the maximum value of σ_I^2 is 3.4 for $\beta = 5.0$, but the peak in intensity variance obtained in the $U = 15.0$ run was 3.9 at screen 12, a little over halfway along the propagation path, where $U = 3.4$. This increase is due to an increase of the ratio

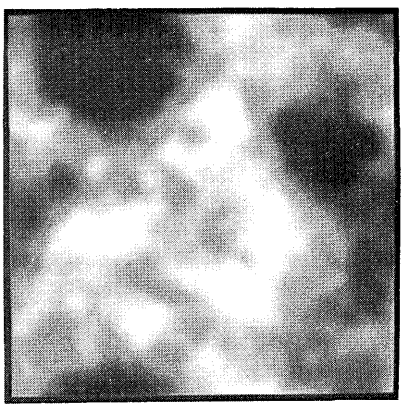

Fig. 7. Sample realization of a phase screen for a power law $\alpha = 1.7$ and an inner scale $\beta = 5.0$. Large-scale variation remains, but small-scale fluctuations are suppressed.

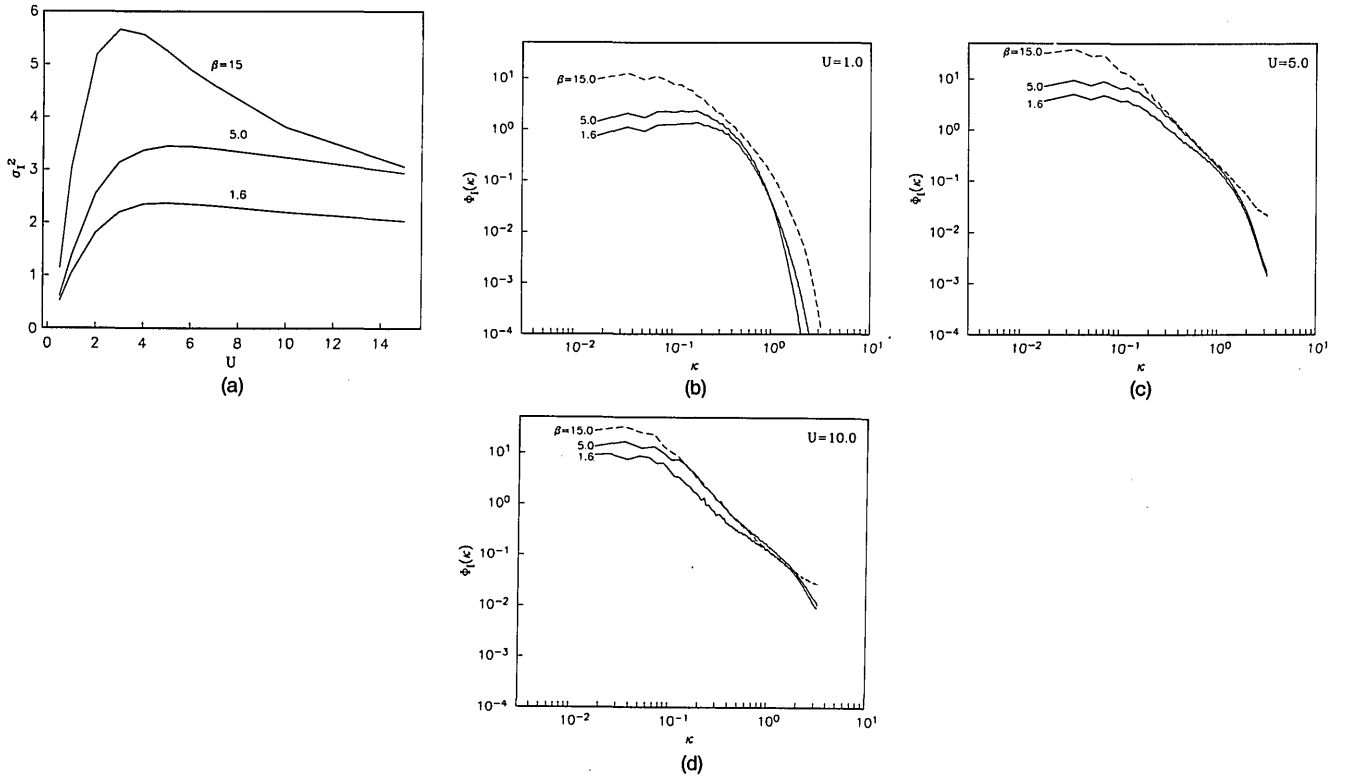

Fig. 8. Intensity statistics for a power law of 1.7 and inner scales of $\beta = 1.6$, 5.0, and 15.0 corresponding to $\beta/R_f = 0.3$, 1, and 3: (a) intensity variance; (b) intensity spectra for $U = 1.0$; (c) $U = 5.0$; and (d) $U = 10.0$.

β/R_f, where R_f in this case is the effective R_f corresponding to the path length from source to observation plane at screen 12. Conversely, for $\beta = 0$, we find the peak value of intensity variance to be the same, regardless of whether U is varied by changing fluctuation strength or path length.

The peak value of σ_I^2 dramatically increases for $\beta \geq R_f$ and also migrates to smaller values of U. The maximum σ_I^2 of 5.5 obtained at $U = 3$ for $\beta/R_f = 3$ is as large as any measured in laser propagation experiments.[29,30] Unfortunately, this value of β/R_f is much too large to be physically reasonable. For $R_f = 1$ cm, this value for β is equivalent to an inner scale of ~9 cm. The maximum value of σ_I^2 is 2.0 for physically reasonable inner scale of about the same size as R_f. Thus we have not explained the large values of measured σ_I^2. One possibility is that a point source may give larger intensity variance than a plane wave source and is a more accurate model of the experimental setup[29]; point source simulation results are not yet available.

Intensity scintillation spatial spectra are shown in Figs. 8(b), (c), and (d) for the same three values of β as above. The effect of the spectral cutoff is apparent in Fig. 8(b) ($U = 1.0$) as a parabolic descent of the power spectrum at high frequencies. Note that even at $U = 1.0$ the $\beta = 15.0$ curve is showing an extended high-frequency region. In weak-scattering conditions this curve would cut off at a lower wavenumber and be underneath the $\beta = 5.0$ curve. This, in addition to the very rapid increase of the $\beta = 15$ intensity variance with U, suggests that an increase in inner scale not only produces an increase in the maximum σ_I^2 but also results in the onset of significant strong scattering effects at lower U values.

The changes noted above in the intensity variance and scintillation spectra, while suggestive, did not prepare us for the striking visual effect produced on the intensity field by increase of the inner scale. Single realizations of the intensity field for $\beta = 5.0$ and $\beta = 15.0$ are shown in Figs. 9 and 10. As in Fig. 6, the three images in each set correspond to U less than, equal to, and greater than that for which the peak in σ_I^2 was obtained. Due to the reduction in screen fine structure, the intensity fields for $U = 1.0$ are much smoother than for the power-law case and clearly show a structure of bright points connected by dimmer lines—a network of caustic surfaces. Maximum values of intensity obtained on the screens of Fig. 10 are 70–170 compared with maxima of 20–80 for the pure power-law screens of Fig. 6, showing the increased efficiency of focusing produced by an increase of inner scale.

Figure 10(a) shows that even for $U = 1.0$, fringes are becoming visible near some of the caustics. At the peak of intensity variance [Figs. 9(b) and 10(b)] interference fringes have become so pronounced they are the dominant feature in the image with up to eight oscillations visible around bright points. A close-up of the fringes is seen around the middle bright area point of Fig. 10(d), which shows the fringe spacing to be approximately the Fresnel length of five samples.

For even stronger scattering conditions, the fringes themselves begin to break up and show intensity varia-

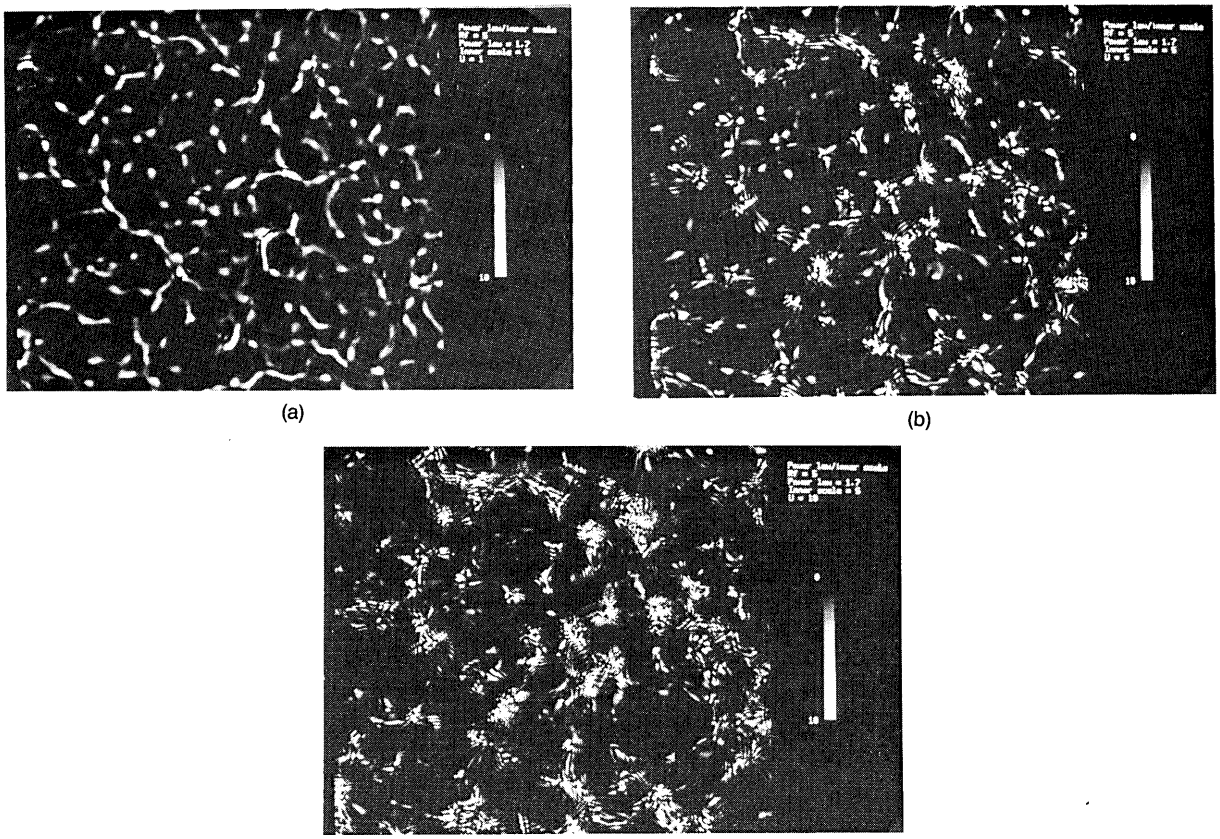

(a) (b) (c)

Fig. 9. Intensity images of a single realization of a power-law medium with $\alpha = 1.7$, $R_f = 5.0$, and $\beta = 5.0$: (a) $U = 1.0$; (b) $U = 5.0$; and (c) $U = 10.0$.

tion in the direction orthogonal to the original direction, producing a checkerboard effect especially visible in the upper left of Fig. 10(e), a close-up of Fig. 10(c). We also note the same growth in the low-frequency structure of islands of brightness surrounded by extended dim regions that was present in the pure power-law case.

Examination of Fig. 8 shows not much aliasing present in any of the spectra corresponding to $\beta = 5.0$ but significant extra high-frequency energy for $\beta = 15.0$ at $U = 10.0$. This indicates that the oscillations at the highest frequencies in Fig. 10(c) (oscillation with a period of two samples) may be exaggerated by a factor of ~ 2. Therefore, the rapid oscillations in the interior of bright regions of Figs. 9(c) and 10(e) may be somewhat spurious, but the fringes at the Fresnel frequency are real. A further striking effect is the relatively large-scale clustering of bright regions for the higher U values [Figs. 6(d), 9(c), 10(c)].

C. Outer Scale

Although a pure power law is often a good approximation to the refractive-index fluctuation spectrum of the medium, it is clear that such a law cannot truly apply for all scales. At some large scale, the power law must give way, if only due to the finite extent of the medium. Such an outer scale L_0 marks the spatial scale boundary in fluid turbulence between the inertial region and the scales at which energy is being fed into the system. The form of the spectrum is dependent on the specific physical processes responsible for the turbulent energy input and thus has no universal description. The standard model which includes the outer scale is that of the von Karman type[1,31]:

$$\Phi_n(\kappa) = K(\alpha) C_n^2 (\kappa^2 + 1/L_0^2)^{-\frac{\alpha}{2}-1}. \quad (25)$$

This form for $\Phi_n(\kappa)$ is employed in theoretical expressions for wave-fluctuation quantities simply to remove divergences. Note that the values for some of these quantities, e.g., phase variance, depend on the value chosen for the outer scale, a very difficult parameter to estimate.

Generally the characteristic maximum size or time interval of the experiment determines an effective outer scale, which then limits the value of divergent quantities.[32] Similarly, simulations are limited by the array size, which in turn limits the total phase variance to a finite value. In this section we investigate the scintillation effects of an outer scale much smaller than the screen size, keeping the power law constant at the Kolomogorov value. A sample phase-screen realization with the above spectrum and $L_0/R_f = 3$ is shown in Fig. 11. It has the same filamentary high-frequency structure seen in the pure power-law case, but less prominent large-scale structures give it a more evenly distributed appearance than Fig. 4.

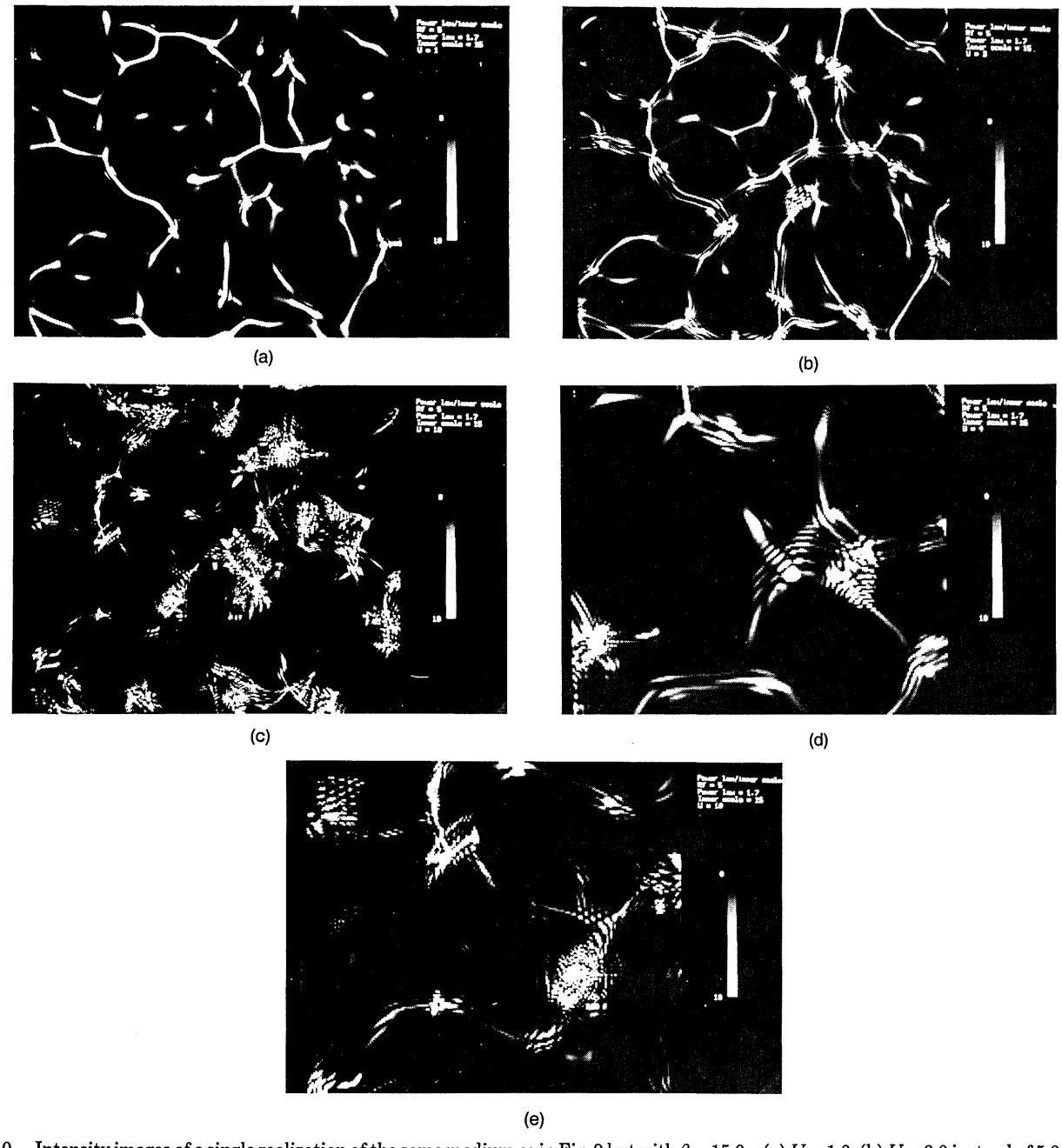

Fig. 10. Intensity images of a single realization of the same medium as in Fig. 9 but with $\beta = 15.0$: (a) $U = 1.0$; (b) $U = 3.0$ instead of 5.0, since the peak in σ_I^2 occurs here; (c) $U = 10.0$; (d) a close-up of the intensity realization for $U = 4.0$ showing a remarkably clear set of fringes emanating from the bright point just to the left of center; and (e) a close-up of (c) showing checkerboard oscillations at the highest spatial frequencies.

Intensity variance as a function of U and L_0 are displayed in Fig. 12(a) for $L_0/R_f = 10$, 3, and 1. Again the parameter C_n^2 is varied to produce the variation of U, keeping the geometry constant. As with the inner scale simulations, when U is varied by changing the propagation distance R, the peak intensity variance is greater than that of Fig. 12(a) due to the increase in L_0/R_f in the region of the peak. For $L_0 = 10R_f$, σ_I^2 results are very nearly identical to those for no explicit outer scale. They differ by <4% over the range of U shown here. As the outer scale is reduced further, the peak in σ_I^2 is further decreased, down to 1.7 for $L_0 = R_f$. The value of U for which the peak occurs is not a function of L_0.

Intensity scintillation spectra for the same values of L_0 as above are shown in Figs. 12(b), (c), and (d) for $U =$ 1, 5, and 10. The effect of smaller outer scales on the intensity spectra is quite pronounced, dramatically reducing low-frequency contributions to the spectrum. As one might expect from a weak-scattering analysis, which is approximately correct at low frequencies, the form of the spectrum is κ^4, independent of the power law, and the spatial frequency for which the spectra at $U = 1$ deviate from the pure power-law form is $\sim 1/L_0$.

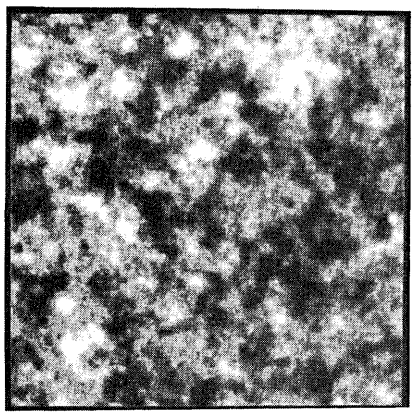

Fig. 11. Sample realization of a phase screen for a power-law $\alpha = 1.7$ and an outer scale $L_0 = 15.0$. Small-scale filamentary structure is similar to Fig. 4, but large-scale variation is suppressed.

In contrast to the inner-scale results, which became very similar to the pure power-law results for large U, the low-frequency structure even at $U = 10$ clearly reflects the effect of the outer scale. This may be explained by noting that asymptotically the low-frequency structure of the intensity spectrum is to first order described by the Rytov result, even when scattering is strong. In these conditions, $\kappa_{\min}$ is increased compared to Eq. (20) because of the outer scale, thus allowing extension of the simulations to larger U than possible for $L_0 > 10R_f$. Of course R_f must also be increased to move the spectral window to higher frequency. We have not done this for the spectra shown here, but we shall in the following section when we show results for a Gaussian spectrum of irregularities.

Sample intensity realizations for $U = 1$, 5, and 10 and $L_0 = 15 = 3R_f$ are shown in Fig. 13. At $U = 1$, Fig. 13(a) shows a filamentary structure more readily than the pure power law of Fig. 6(b) but not as clearly as Fig. 9(a) ($\beta = 5$). Overall less contrast is visible in the intensity variations of Fig. 13(a) than either Fig 6(b) or 9(a). As the scattering strength is increased, fringes become visible in a manner similar to the pure power-law result but with less strong clustering. At $U = 10$, the small-scale structure is similar to the pure power law. The decrease in spectral strength at low frequencies manifests itself as a decrease in the scale of clustering (on the average) and in the magnitude of variations; e.g., the dark areas are significantly reduced in size in Fig. 13(c) compared with Fig. 6(d). Thus the large-scale structure of the medium is reflected in the clustering structure of the bright and dark areas in the observing plane.

D. Single-Scale Medium

Although it does not apparently reflect the true structure of any natural medium, the single-scale Gaussian spectrum has often been the spectrum of choice[14,33,34] for tractability in theoretical analysis:

$$\Phi_n(\kappa) = C_n^2 \exp(-\kappa^2 L^2/4), \tag{26}$$

where L is the single scale characterizing the medium. A sample Gaussian phase screen is shown in Fig. 14 for $L = 16$. It is very smooth in appearance, even compared with the inner-scale model of Fig. 7, and of

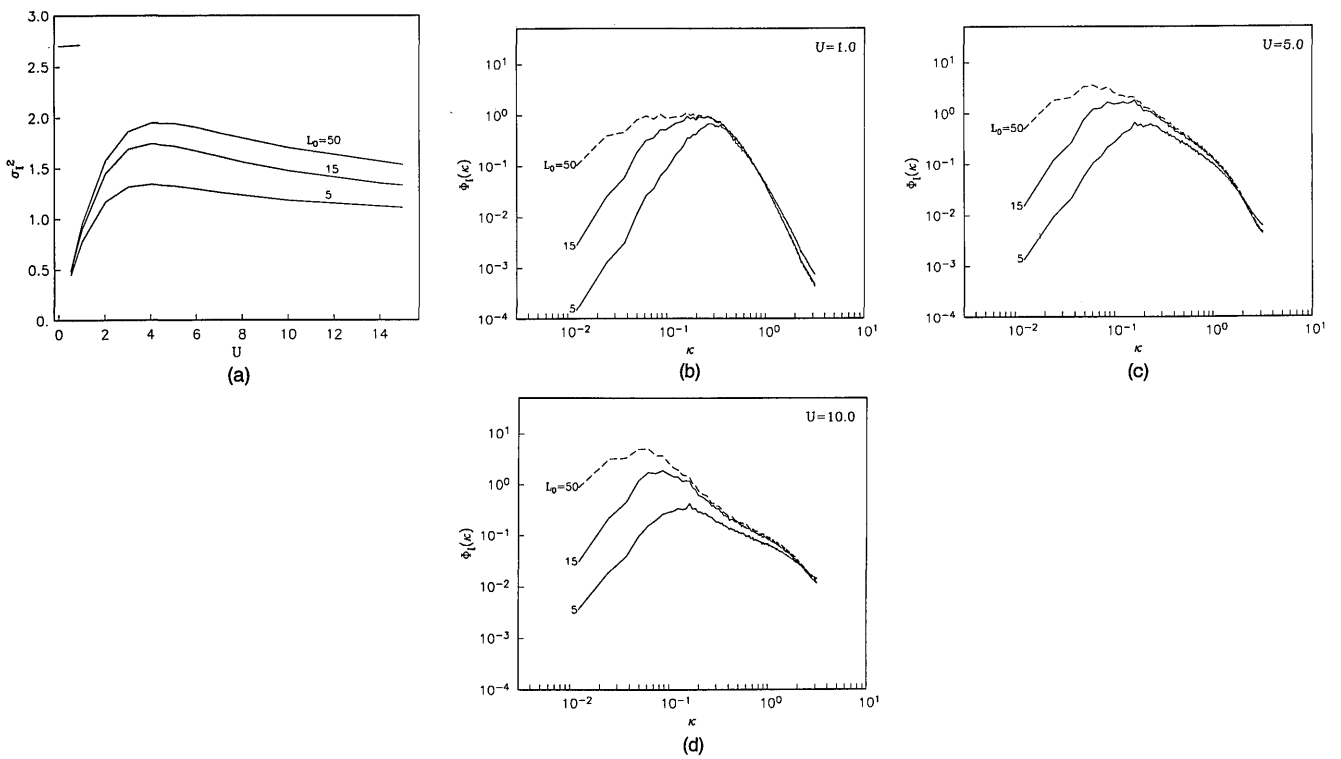

Fig. 12. Intensity statistics for a power-law medium with $\alpha = 1.7$, outer scales of 5, 15, and 50, and $R_f = 5.0$: (a) intensity variance as a function of scattering strength U; (b) intensity spectra for $U = 1.0$; (c) $U = 5.0$; and (d) $U = 10.0$. Spectra for all strengths of scatter show a substantial effect at low frequencies from the outer scale.

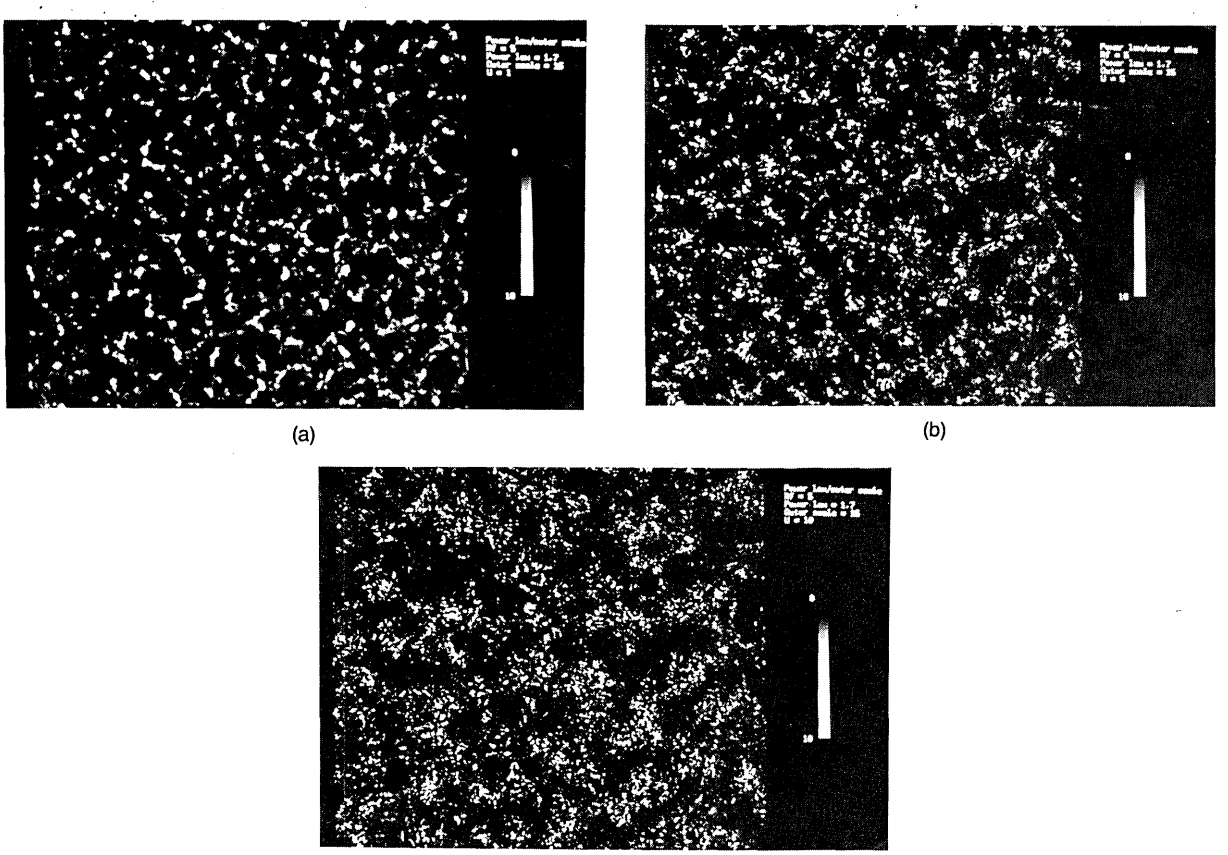

Fig. 13. Intensity images of a single realization of a power-law medium with $\alpha = 1.7$, $R_f = 5.0$, and $L_0 = 15.0$: (a) $U = 1.0$, (b) $U = 5.0$, and (c) $U = 10.0$.

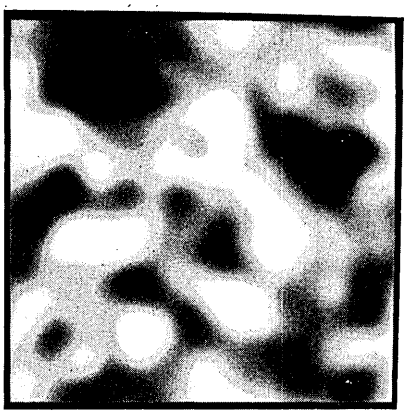

Fig. 14. Sample realization of a phase screen for a (single-scale) Gaussian medium with scale $L = 16$. In this case both large- and small-scale structures are suppressed relative to the pure power law of Fig. 4.

course has less energy at the largest scales. Due to this narrow energy bandwidth, the Gaussian spectrum allows simulation to much greater values of U than power-law media. We have taken advantage of this property, and in Fig. 15(a) we show the dependence of σ_I^2 on U from $U = 0$ to $U = 50$ for $L/R_f = 1.6$ and $L/R_f = 0.8$. If $L > R_f$ there is some focusing, producing an increase in the peak value of σ_I^2, but the lack of large-scale fluctuations produces a result which is 25% less than that for $\beta/R_f = 1$. When $L < R_f$, focusing is not strong, with a peak σ_I^2 of only 1.2.

One can regard a Gaussian spectrum as a collapsed power-law spectrum with inner and outer scales equal, so both inner and outer scale effects modify the scattering; i.e., a large inner scale tends to increase the scintillations by allowing more precise focusing, while a small outer scale tends to decrease the scintillations by suppressing the strength of the large-scale focusing structures. It is clear from the results of Fig. 15(a) that the outer-scale effect is dominant when $L < R_f$ and indeed is very effective at reducing the intensity variance even when the medium scale is larger than the Fresnel scale, when one, on the basis of experience with the effect of inner scale on power-law spectra, would expect very efficient focusing and a large peak value for σ_I^2.

We note that, even when we are able to simulate $U = 50$, the intensity variance has still not returned to unity, and its approach to that asymptotic value is very slow indeed.

Intensity spectra for $U = 1$, 5, and 40 are shown in Fig. 15(b) for $L/R_f = 1.6$. The separation of scales also occurs quite slowly with U compared to power-law media.

Finally, Figs. 16(a)–(d) contain images of one intensity realization for $U = 1, 5, 10$, and 40. The maximum

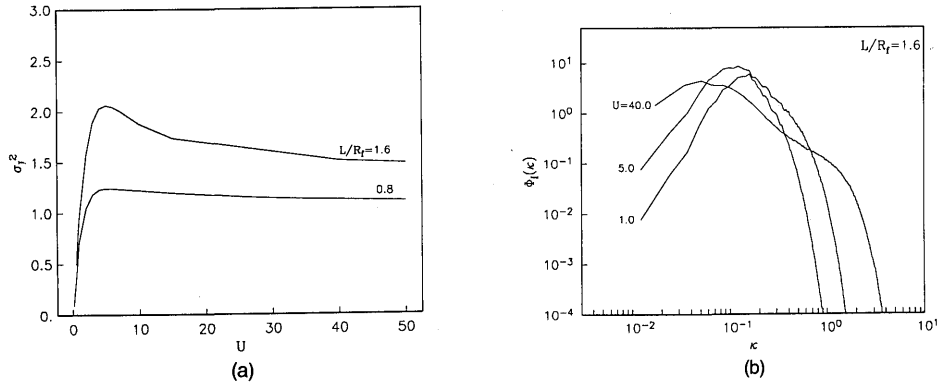

Fig. 15. Intensity statistics for a Gaussian medium with varying scale size: (a) intensity variance as a function of scattering strength U for L_0/R_f of 1.6 and 0.8 showing the increase in peak value of σ_I^2 when the scale size becomes greater than the Fresnel length and (b) intensity spectra for $U = 1.0$, 5.0, and 40.0. Note that essentially no aliasing is encountered even at $U = 40.0$ due to the narrow bandwidth of the Gaussian medium spectrum. κ_{min} and κ_{max} do separate but much more slowly than for a power-law medium.

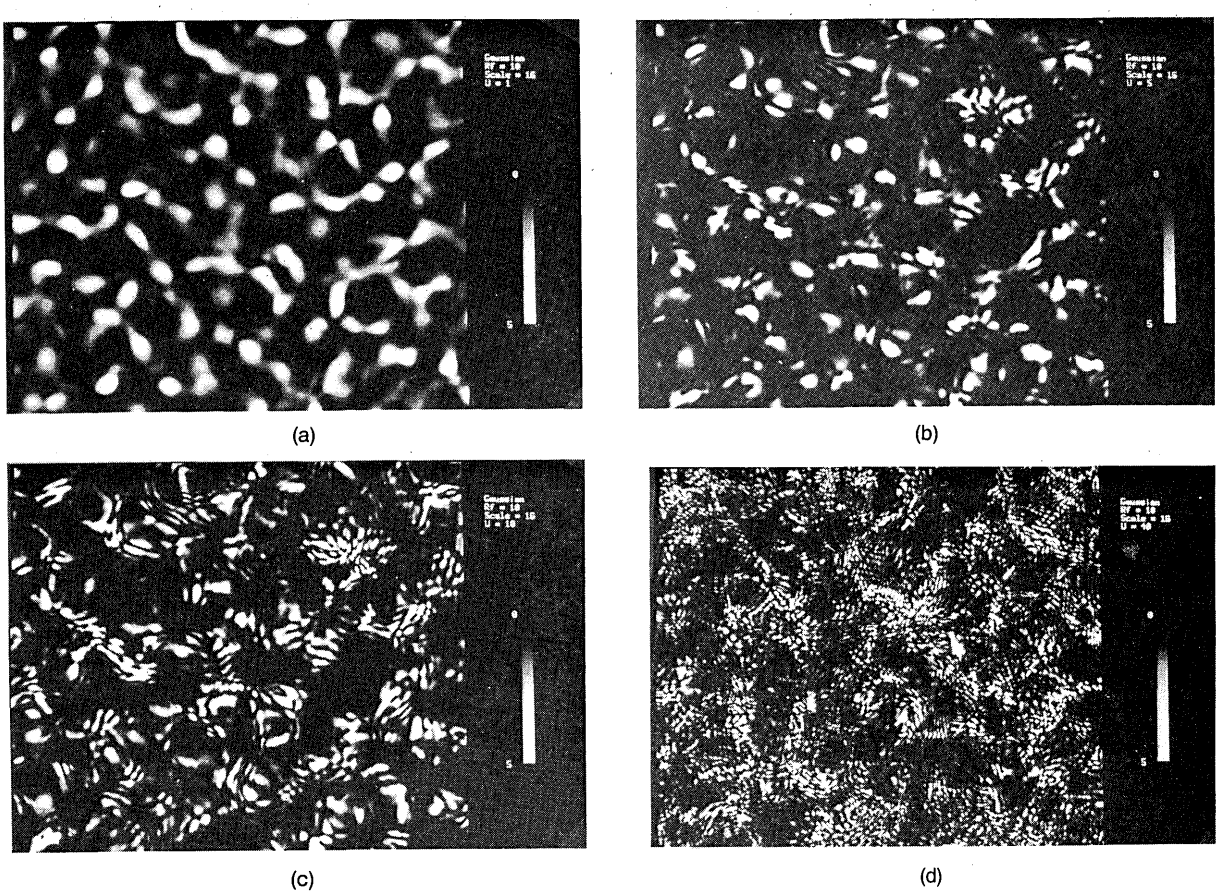

Fig. 16. Intensity images of a single realization of a (single-scale) Gaussian medium with $L = 16.0$, $R_f = 10.0$: (a) $U = 1.0$; (b) $U = 5.0$ (the peak); (c) $U = 10.0$ (past the peak); and (d) $U = 40.0$. Intensity range is 0–5 for these images to enhance the detail.

values of intensity for these realizations are much lower than those for the power-law media, so we have decreased the intensity cutoff value to 5 instead of 10. This allows the structure of the intensity scintillations to be seen more easily. The progression of images shows clearly the decrease in the coherence length of the intensity fluctuations with increasing U and the development of caustic regions and interference fringes.

IV. Comparison with Analytic Approximations

In this section we compare intensity variance results from simulations with approximate theoretical calculations of Whitman and Beran[5] (WB) and investigate a suggestion of Booker *et al.*[11] that extended media may be modeled approximately by a single screen with appropriate strength and position.

A two-scale technique has been used by Macaskill[4] and Frankenthal *et al.*[35] to solve the fourth moment equation in the transform domain and obtain a series solution for $\Phi_I(\kappa)$ valid for all κ. WB show that this solution is valid for all strengths of scattering and calculate intensity variance for plane wave propagation through 2-D and 3-D power-law media with nonzero inner scale. Intensity standard-deviation results for propagation through a 3-D medium as a function of σ_1 are shown in Fig. 17 (reproduced from WB, Fig. 4). To compare with simulation results, we relate the parameters of the WB calculation to simulation parameters.

The WB parameter $\gamma_K = k^3 C_n^2 \beta^{11/3}$, which is the ratio of the inner scale β to a scattering scale determined by the wavelength and the strength of fluctuations, is constant for each WB curve in Fig. 17. Thus, for constant k the medium must also be constant in its properties (C_n^2 and β), and the variation of σ_1 stems from variation in R, the propagation distance. In terms of the simulation parameters

$$\gamma_\kappa = 6.6098 \left(\frac{C_1 \beta^{11/3}}{r_f} \right), \tag{27}$$

$$\sigma_1 = 2.4377 N^{11/12} r_f^{5/6} C_1^{1/2}, \tag{28}$$

where N is the number of screens through which the wave propagates. If $\sigma_1 = 4$ for $N = 20$ and $r_f = 1.1209$, then $C_1 = 0.0092$, and for $\gamma_K = 10$, $\beta = 4.2$ and $\beta/R_f = 0.83$. The values of σ_1 for which the peak in intensity standard deviation occurs are almost identical for both WB and our simulations, but the simulation results, shown by dashed lines in Fig. 17, are greater than the WB calculations by 15%, an intensity variance difference of ~25%. This difference is likely due to the use of only the first term in the expansion for the WB theory. Inclusion of higher terms would probably result in better agreement.

Comparing numerical solutions for 2-D wave propagation through an extended random medium and through a thin screen of the same total phase variance placed in the center of the medium, Booker *et al.*[11] find that very similar results are obtained for intensity correlation functions. The inner scale was not explic-

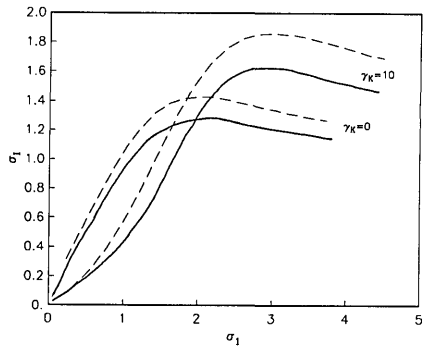

Fig. 17. Comparison of intensity standard deviation computed by WB (solid lines) with simulation results (dashed lines) for 3-D power-law spectrum with inner scale ($\gamma_K = 10$) and pure power law ($\gamma_K = 0$). The strength parameter σ_1 is varied by change in propagation distance, not strength of fluctuations.

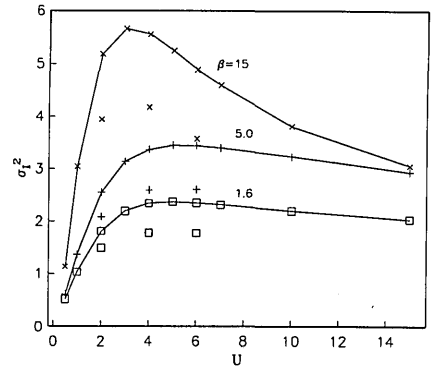

Fig. 18. Comparison of simulation intensity variance results for an extended medium (continuous curve) with those of the equivalent thin screen model (symbols) of Booker *et al.* at $U = 2$, 4, and 6. The medium spectrum has a Kolmogorov power law with inner scale: $\beta/R_f = 0.3$, 1.0, and 3.0 (boxes, pluses, and crosses, respectively).

itly included in the calculation, the nonzero sampling interval providing an inner scale of $\sim 0.05 R_f$.

We investigate the usefulness of this approximation in full 3-D scattering with inner scales nearer the Fresnel length in size. We compare a 20-screen extended medium simulation to a single-screen simulation with 20 times the strength and half of the path length. Inner scales of 1.6, 5, and 15 samples were considered at $U = 2$, 4, and 6, the region around the intensity variance peak. Results of this comparison are shown in Fig. 18: the thin screen results are 25% lower than the extended medium results in all cases.

It is clear that the basic behavior of σ_I^2 as a function of U is reproduced by the single-screen representation, but the result is not as quantitatively accurate in three dimensions with an inner scale present as it is in two dimensions. If the spectra are examined, we find they look very similar with only relatively subtle differences (Fig. 19). High frequencies show very good agreement, low frequencies somewhat less; the major source of the difference in σ_I^2 is in the transition region between the low and high frequencies, around the Fresnel frequency. It has been suggested that in strong

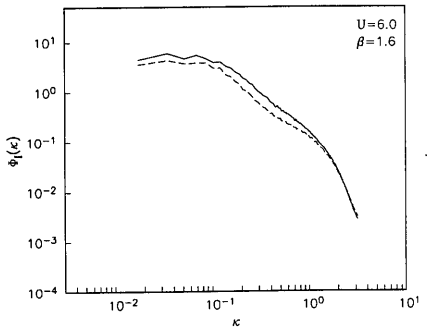

Fig. 19. Intensity spectra for extended medium simulation (solid curve) vs single equivalent screen (dashed curve) for $U = 6$ and $\beta = 1.6$.

scatter with finite inner scale, substantial contributions to the intensity variance are made by portions of the medium near the observing plane (Frehlich, 1986), and such effects cannot be duplicated by an equivalent thin screen.

V. Conclusions

We have simulated the propagation of plane waves through extended 3-D random media using a multiple phase screen technique. Limits of applicability were found to be mainly due to the increasing bandwidth of the spatial spectrum of intensity fluctuations exceeding the finite bandwidth available in the simulation grid. We find that for a 512×512 grid, the maximum U is ~ 15. A variety of medium spectra were considered: pure power law, inner scale, outer scale, and single scale (Gaussian). Intensity variance, intensity spectra, and images of single realizations of intensity at the observation plane were presented for all these media, and morphology of the results is described.

We have shown that these simulations can be useful in evaluating the accuracy of theoretical approximation in the strong focusing region where the number of terms required for an accurate solution is unknown. They should also be useful in evaluating the scattering properties of complex and spatially dependent media in strong scattering conditions.

The results for finite inner scales show an enhancement of intensity variance with increasing β, but $\beta = 3R_f$ is required to duplicate the extreme values of σ_I^2 obtained in experiments. This inner scale is almost 10 times the accepted value expected in the atmosphere, so plane wave propagation may not properly describe the experimental conditions. A point source is a more appropriate model for the experiment, and there may be a substantial quantitative difference between plane wave and point source results. Our simulation includes all the essential known physics of the problem, except the source structure; if the point source simulation fails to agree with experimental results, our model for the atmospheric medium fluctuations has to be modified.

Previous calculations have concentrated exclusively on statistical quantities such as correlation functions and spectra. We have shown that these do not contain all the information present in the intensity realizations, and examination of specific realizations of the intensity field reveals features which may provide additional insight. For example, it is clear from the images that under weak scattering the small-scale Fresnel length structure of the medium dominates the intensity scattering pattern. As the strength of scattering increases, caustics and interference fringes begin to form. Finally, in still stronger scatter, the clustering of bright points begins to reflect the large-scale structure of the medium.

This work was supported by DARPA grant MDA903-86-K-0010 and the San Diego Supercomputer Center.

References

1. V. I. Tatarski, "The Effects of the Turbulent Atmosphere on Wave Propagation," National Technical Information Service, TT-68-50464 (1971).
2. J. L. Codona, D. B. Creamer, S. M. Flatté, R. G. Frehlich, and F. S. Henyey, "Solution for the Fourth Moment of Waves Propagating in Random Media," Radio Sci. **21,** 929 (1986).
3. R. L. Fante, "Electric Field Spectrum and Intensity Covariance of a Wave in a Random Medium," Radio Sci. **10,** 77 (1975).
4. C. Macaskill, "An Improved Solution to the Fourth Moment Equation for Intensity Fluctuations," Proc. R. Soc. London Ser. A **386,** 461 (1983).
5. A. M. Whitman and M. J. Beran, "Two-Scale Solution for Atmospheric Scintillation," J. Opt. Soc. Am. A **2,** 2133 (1985).
6. S. M. Flatté and F. D. Tappert, "Calculation of the Effect of Internal Waves on Oceanic Sound Transmission," J. Acoust. Soc. Am. **58,** 1151 (1975).
7. C. Macaskill and T. E. Ewart, "Computer Simulation of Two-Dimensional Random Wave Propagation," IMA J. Appl. Math. **33,** 1 (1984).
8. R. Buckley, "Diffraction by a Random Phase-Changing Screen: A Numerical Experiment," J. Atmos. Terr. Phys. **37,** 1431 (1975).
9. C. L. Rino and J. Owen, "Numerical Simulations of Intensity Scintillation Using the Power Law Phase Screen Model," Radio Sci. **15,** 41 (1980).
10. J. P. Filice, "Studies of the Microscale Density Fluctuations in the Solar Wind Using Interplanetary Scintillations," U. California, San Diego, Ph.D. Thesis (1984).
11. H. G. Booker, J. A. Ferguson, and H. O. Vats, "Comparison between the Extended-Medium and the Phase-Screen Scintillation Theories," J. Atmos. Terr. Phys. **47,** 381 (1985).
12. V. A. Fock, "Theory of Radio-Wave Propagation in an Inhomogeneous Atmosphere for a Raised Source," Bull. Acad. Sci. URSS Ser. Phys. **14,** 70 (1950).
13. S. M. Flatté, R. Dashen, W. H. Munk, K. M. Watson, and F. Zachariasen, *Sound Transmission Through a Fluctuating Ocean* (Cambridge U.P., London, 1979).
14. R. Dashen, "Path Integrals for Waves in Random Media," J. Math. Phys. **20,** 894 (1979).
15. B. J. Uscinski, "Analytical Solution of the Fourth-Moment Equation and Interpretation as a Set of Phase Screens," J. Opt. Soc. Am. A **2,** 2077 (1985).
16. D. L. Knepp, "Multiple Phase-Screen Calculation of the Temporal Behavior of Stochastic Waves," Proc. IEEE **71,** 722 (1983).
17. R. L. Fante, "Inner-Scale Size Effect on the Scintillations of Light in the Turbulent Atmosphere," J. Opt. Soc. Am. **73,** 277 (1983).
18. V. R. Rumsey, "Scintillations due to a Concentrated Layer with a Power-Law Turbulence Spectrum," Radio Sci. **10,** 107 (1975).

19. K. S. Goshelashvily and V. I. Shishov, "Saturated Fluctuations in the Laser Radiation Intensity in a Turbulent Medium," Sov. Phys. JETP **39**, 605 (1974).
20. R. G. Frehlich, "Intensity Covariance of a Point Source in a Random Medium with a Kolmogorov Spectrum and an Inner Scale of Turbulence," J. Opt. Soc. Am. A **4**, 360 (1987).
21. R. Esswein and S. M. Flatté, "Calculation of the Phase-Structure Function Density from Oceanic Internal Waves," J. Acoust. Soc. Am. **70**, 1387 (1981).
22. R. G. Frehlich, "Laser Propagation in Random Media," U. California, San Diego, Ph.D. Thesis (1982).
23. K. S. Goshelashvily and V. I. Shishov, "Saturation of Laser Irradiance Fluctuations beyond a Turbulent Layer," Opt. Quantum Electron. **7**, 524 (1975).
24. D. P. Hinson, "Strong Scintillations during Atmospheric Occultations: Theoretical Intensity Spectra," Radio Sci. **21**, 257 (1986).
25. R. Woo and J. W. Armstrong, "Spacecraft Radio Scattering Observations of the Power Spectrum of Electron Density Fluctuations in the Solar Wind," J. Geophys. Res. **84**, 7288 (1979).
26. R. J. Hill and S. F. Clifford, "Theory of Saturation of Optical Scintillation by Strong Turbulence for Arbitrary Refractive-Index Spectra," J. Opt. Soc. Am. **71**, 675 (1981).
27. R. J. Hill, "Spectra of Fluctuations in Refractivity, Temperature, Humidity, and the Temperature-Humidity Cospectrum in the Inertial and Dissipation Ranges," Radio Sci. **13**, 953 (1978).
28. R. J. Hill, "Theory of Saturation of Optical Scintillation by Strong Turbulence: Plane-Wave Variance and Covariance and Spherical Wave Covariance," J. Opt. Soc. Am. **72**, 212 (1982).
29. W. R. Coles and R. G. Frehlich, "Simultaneous Measurements of Angular Scattering and Intensity Scintillation in the Atmosphere," J. Opt. Soc. Am. **72**, 1042 (1982).
30. R. L. Phillips and L. C. Andrews, "Measured Statistics of Laser-Light Scattering in Atmospheric Turbulence," J. Opt. Soc. Am. **71**, 1440 (1981).
31. J. W. Goodman, *Statistical Optics* (Wiley-Interscience, New York, 1985).
32. C. L. Rino, "A Power Law Phase Screen Model for Ionospheric Scintillation 1. Weak Scatter," Radio Sci. **14**, 1135 (1979).
33. B. J. Uscinski, C. Macaskill, and M. Spivack, "Path Integrals for Wave Intensity Fluctuations in Random Media," J. Sound Vib. **106**, 509 (1986).
34. E. E. Salpeter, "Interplanetary Scintillations. I. Theory," Astrophys. J. **147**, 433 (1967).
35. S. Frankenthal, A. M. Whitman, and M. J. Beran, "Two-Scale Solutions for Intensity Fluctuations in Strong Scattering," J. Opt. Soc. Am. A **1**, 585 (1984).

Meetings *continued from page 2110*

1988
June

14–19 China Optoelectronics Laser '88, Beijing *Cahners Expo. Group, P.O. Box 70007, Wash., DC 20088*

15–16 Fiber Optics in Plain English Sem., Atlanta *Trellis Communications Corp., 5 Manor Pkwy., Salem, NH 03079*

15–17 **Spatial Light Modulators & Applications Mtg.,** Lake Tahoe *OSA Mtgs. Dept., 1816 Jefferson Pl., NW, Wash., DC 20036*

17–5 July 1988 Summer Inst., History & Philosophy of Sci., Berlin *W. Woodward, Dept. Psych., Conant Hall, U. New Hampshire, Durham, NH 03824*

20–22 18th Power Modular Symp., Hilton Head *IEEE, 345 E. 47th St., New York, NY 10017*

20–23 10th Symp. on Thermophysical Properties, Gaithersburg *A. Cezairliyan, Rm. 124 Hazards Bldg., NBS, Gaithersburg, MD 20899*

20–24 14th Int. Laser Radar Conf., San Candido *L. Stefanutti, IROE, CNR, Via Panciatichi, 64-50127 Firenze, Italy*

20–24 Fluid Mechanics Measurement course, Minneapolis *J. Becker, U. of MN, Professional Dev., 107 Armory, 15 Church St. S.E., Minneapolis, MN 55455*

20–24 Advanced Infrared Technology course, Ann Arbor *Eng. Summer Confs., U. of MI, Chrysler Ctr./N. Campus, Ann Arbor, MI 48109*

20–24 Optical Thin Film Coating Technology course, Rochester *J. Reiter, Inst. of Optics, U. of Rochester, Rochester, NY 14627*

20–1 July Contemporary Optics course, Rochester *J. Reiter, Inst. of Optics, U. of Rochester, Rochester, NY 14627*

21–22 Fiber Optics in Plain English Sem., Anaheim *Trellis Communications Corp., 5 Manor Pkwy., Salem, NH 03079*

22–24 Medical Laser Safety Officers course, Cincinnati *Laser Inst. Amer., 5151 Monroe St., Toledo, OH 43623*

24–29 5th Conf. Australian Optical Soc., Sydney *AOS Dept. Theoretical Phys., U. Sydney, 2006, Australia*

26–29 Photochemistry for Imaging Symp., Minneapolis *SPSE, 7003 Kilworth Lane, Springfield, VA 22151*

26–30 Engineering & Industrial Sensing for Advanced Manufacturing Technologies Mtg., Dearborn *SPIE, P.O. Box 10, Bellingham, WA 98227*

27–30 Color: The Educator in Art & Design Sem., New York *ISCC-Sem. Dept., Fashion Inst. of Tech., 7th Ave. & 27th St., New York, NY 10001*

27–30 Ultrafast Optics & Optoelectronics course, Rochester *J. Reiter, Inst. of Optics, U. of Rochester, Rochester, NY 14627*

27–1 July Lens Design course, Rochester *J. Reiter, Inst. of Optics, U. of Rochester, Rochester, NY 14627*

27–1 July Fiber Optics for Avionics Systems course, El Segundo *UCLA Ext., P.O. Box 24901, Los Angeles, CA 90024*

continued on page 2156